The Astrophysical Journal, 975:248 (9pp), 2024 November 10 https://doi.org/10.3847/1538-4357/ad83bb

Exploring Spatial and Temporal Patterns in the Debrecen Solar Faculae Database: Part II

Marianna B. Korsós[1,2,3], Anett Elek[4,3], Francesca Zuccarello[5,6], and Robertus Erdélyi[2,3,7]

[1] University of Sheffield, Department of Automatic Control and Systems Engineering, Amy Johnson Building, Portobello Street, Sheffield S1 3JD, UK; komabi@gmail.com
[2] Department of Astronomy, Eötvös Loránd University, Pázmány Péter sétány 1/A, H-1112 Budapest, Hungary
[3] Gyula Bay Zoltán Solar Observatory (GSO), Hungarian Solar Physics Foundation (HSPF), Petőfi tér 3, H-5700 Gyula, Hungary
[4] University of Debrecen, Egyetem tér 1, H-4032 Debrecen, Hungary
[5] Dipartimento di Fisica e Astronomia "Ettore Majorana," Università di Catania, Via S. Sofia 78, I-95123 Catania, Italy
[6] INAF—Catania Astrophysical Observatory, Via S. Sofia 78, I-95123 Catania, Italy
[7] Solar Physics and Space Plasma Research Centre, School of Mathematics and Statistics, University of Sheffield, S3 7RH, UK

Received 2024 March 18; revised 2024 October 1; accepted 2024 October 4; published 2024 November 7

Abstract

In this study, utilizing data from the Solar Dynamics Observatory/Helioseismic and Magnetic Imager–Debrecen Faculae Data Catalogue, we investigated solar facula distribution over timescales much larger than the individual lifetimes of faculae. We aimed to better comprehend the behavior of the Sun's global magnetic field, where faculae play a role as markers. (1) Along the latitudinal direction, we observed the following in the appearance of faculae. (i) Short-term periods with the Carrington rotation (27.3 days) and some of its harmonics (approximately 13.5 and 9 day periods) are identified. In the northern hemisphere, there is also a faint 7 day period. (ii) We also identified longer periods. These longer periods, approximately between 150–300 and 300–500 days, exhibit a diminishing trend from the solar equator to the poles in both hemispheres. (2) Analyzing the distribution and evolution of the longitudinal coordinates of the faculae, we identified two pairs of active longitudes that are separated by 180° from each other.

Unified Astronomy Thesaurus concepts: Solar faculae (1494)

1. Introduction

One of the enigmatic and also intriguing features of solar magnetic activity is its spatiotemporal organization, which spans multiple scales from days to decades. The most prominent and at the same time well known is the widely documented 11 yr Schwabe cycle (H. Schwabe & H. Schwabe 1844), characterized by the periodic variations in sunspot numbers over time. Spatially, sunspot activity not only follows the latitudinal migration illustrated by the butterfly diagram but is also claimed to show a propensity for active regions to cluster at preferential longitudes, known as active longitudes. The concept of active longitudes on the Sun has been a subject of thorough investigation since the early twentieth century, with interesting suggestions and contributions from researchers like H. M. Losh (1939), R. S. Bogart (1982), L. Zhang et al. (2011), and others. Active longitude studies have consistently proposed that various indicators of solar activity, including sunspots (S. V. Berdyugina & I. G. Usoskin 2003; I. G. Usoskin et al. 2005; D. A. Juckett 2006), the solar global magnetic field (E. E. Benevolenskaya et al. 1999; V. Bumba et al. 2000), the heliospheric magnetic field (A. Ruzmaikin et al. 2001; K. Mursula & T. Hiltula 2004), and solar flares (T. Bai 1988, 2003; N. Gyenge et al. 2016), all exhibit a marked preference for occurring at certain longitude ranges; hence the notion of active longitude.

Nevertheless, discrepancies have been reported in the lifetimes and rotation rates of active longitudes when comparing different solar-activity markers. For instance, H. Balthasar (2007) observed variations in the rotation periods of sunspots over long timescales by examining sunspot records from 1818 to 2006. D. Heristchi & Z. Mouradian (2009) detected an acceleration in the rotation rate from solar cycles 19 to 23 through an analysis of sunspot numbers and coronal radio flux at 10.7 cm. Further, several researchers have suggested a gradual fading of the propensity for sunspot groups to be aggregate at specific longitudes over time, with the most enduring correlations spanning 10–15 Carrington rotations (CR; M. J. M. Castenmiller et al. 1986; G. de Toma et al. 2000; J. Pelt et al. 2010; I. G. Kostyuchenko & E. S. Vernova 2024, and references cited therein, and many others). The active longitudes are approximately 20°–60° wide, as observed and argued for by, e.g., V. Bumba & R. Howard (1969), N. Gyenge et al. (2014), and N. Gyenge et al. (2016). V. Gaizauskas et al. (1983) also noted that complexes of solar activity in these active longitudes are sustained by the frequent emergence of new magnetic fluxes. However, the underlying causes of these spatiotemporal patterns still remain a subject of debate. In fact, there are even a few who argue that active longitude may not exist. On the theory side, to the best of our knowledge, there is no dynamo theory available yet that is able to account for or predict the presence of the active longitude. A real bottleneck seems to be the needed computational power to carry out three-dimensional simulations where full rotational (magnetic) symmetry is relaxed.

Recently, A. Elek et al. (2024) conducted a comprehensive analysis of the presence of active longitudes employing heliographic data of solar faculae. They observed a pattern of alternating stronger and weaker facula bands at given sets of longitudes. The presence of these alternating bands suggests a link between the existence of faculae and the contentious

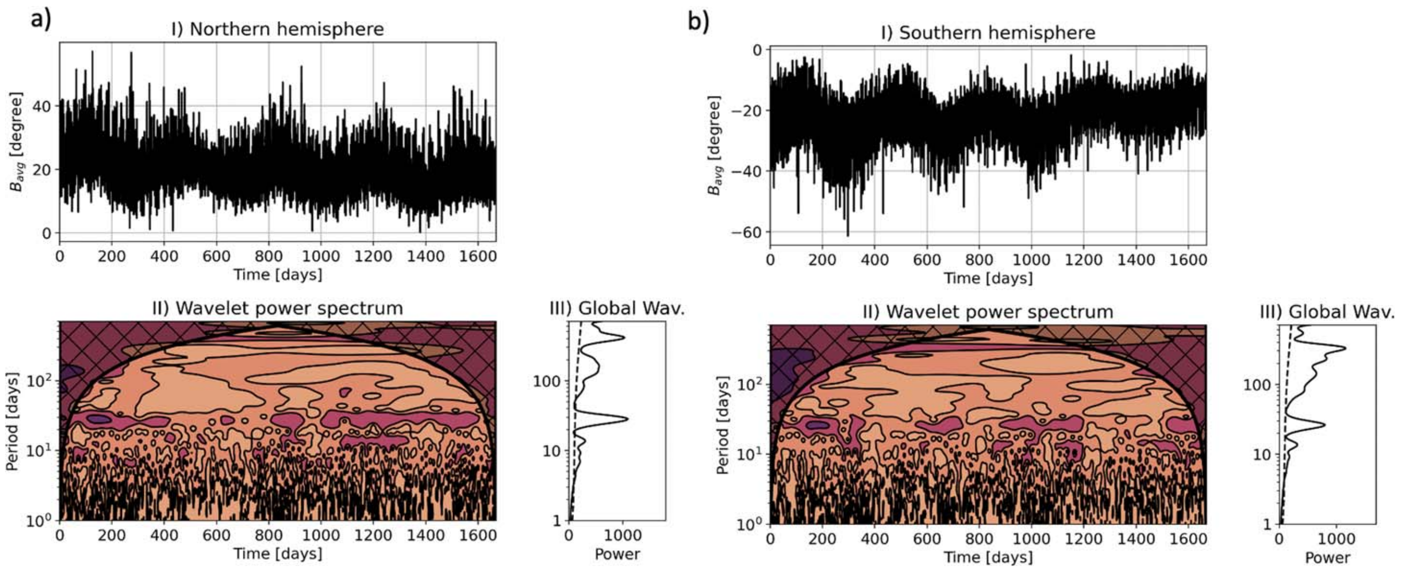

Figure 1. Panels (a) and (b) refer to the analysis of the calculated average latitude value B_{avg} on the northern and southern hemispheres, respectively. Subpanels (I)(a) and (b) show the evolution of the B_{avg} on the respective hemispheres. Subpanels (II)(a) and (b) are the wavelet power spectra of the corresponding time series. The x-axis of each wavelet power spectrum denotes the time of the data, and the y-axis is the period. In the wavelet power spectrum plots, the hatched black lines bound the cone of influence. The black contours enclose regions that are greater than the 2σ confidence level for a white-noise process. Subpanels (III)(a) and (b) to the right of each wavelet power spectrum are the corresponding global wavelet spectra with the power averaged over time. The black dashed lines mark the 2σ confidence level in these global wavelet spectra. The periods are measured in days.

concept of active longitude. A. Elek et al. (2024) bolstered this theory through both a visual heuristic model and additional advanced dynamo simulations, which underscore the interpretation of the solar active longitude phenomena (for more details, please see the ends of Sections 3 and 5 in A. Elek et al. 2024). They also briefly discussed some identified periods that were estimated by fast Fourier transformation. However, these periods were not examined in more detail.

Therefore, our study aims now to delve into the potential correlation between active longitude and various solar global temporal variations (i.e., oscillations) of the heliographic loci observed in solar facula data. In this regard, our research builds upon and expands the work of A. Elek et al. (2024).

The following sections provide details of our analysis in this work. In Section 2, we introduce the data used in our study. Sections 3 and 4 outline our data-processing methodology, including the procedure for determining the periods of oscillations in the latitudinal direction from solar south to north. In Section 5, we discuss the identified active longitudes and active nests in the facula data. Finally, Section 6 summarizes our conclusions.

2. Database

In line with the research conducted by A. Elek et al. (2024), we employed the Solar Dynamics Observatory (SDO)/Helioseismic and Magnetic Imager–Debrecen Faculae Data Catalogue (HMIDD), spanning from 2010 May 1 to 2014 December 31 (T. Baranyi et al. 2016).

In the HMIDD catalog, the white-light faculae were identified using the Sunspot Automatic Measurement (SAM; L. Györi 1998) software package. The SAM utilizes data from the Helioseismic and Magnetic Imager onboard the SDO, identifying the faculae in a continuum image, based on an intensity threshold and the minimum measured pixel area as determined by the resolution reported by B. Bovelet & E. Wiehr (2001). Subsequently, the SAM aligns the continuum image with the corresponding magnetogram to calculate the average magnetic field strength within the contoured area. For each identified facula contour, the heliographic coordinates are calculated as the centroid of the group of pixels within the contour. Finally, the HMIDD includes details such as observation date and time, dimensions, and solar coordinates in Carrington coordinates (latitude B, longitude L) for each facula, along with the average magnetic field strength within these regions, recorded hourly.

To align with the data-selection criteria of A. Elek et al. (2024), we excluded faculae located near the Sun's visible disk periphery. Our analysis concentrates on faculae within $|\pm 70|^{\circ}$ of the longitudinal distance from the Sun's central meridian, with magnetic field strengths between −500 and 500 G. We adhere to a threshold of $|500|$ G for facular magnetic field values, a limit supported by literature indicating that such regions typically exhibit a spatially averaged field strength of up to $|500|$ G (E. N. Frazier 1971; A. M. Title et al. 1992).

3. Time-series Analyses of Averaged Latitudes of Solar Faculae in the Northern and Southern Hemispheres

To thoroughly investigate possible oscillatory patterns in the HMIDD solar facula data set during the observation interval, we analyzed data taken every 2 hr from the HMIDD catalog. First, we calculated the average Carrington latitude (B_{avg}) of all faculae in each hemisphere—north and south—every 2 hr. The time series of the obtained average latitude B_{avg} are displayed in subpanel (I) of Figures 1(a) and (b), respectively. This method allows for an examination of the evolution of B_{avg} over the approximately four-year observation period and aids in identifying any hemispheric differences.

Upon an initial quick examination, one can identify even visually some periodic patterns in the two hemispheric B_{avg} time series. The periodic patterns found in the averaged latitudinal coordinates of faculae we refer to as global latitudinal oscillations (GLOs). To further explore these periods

Table 1
Periods Found by Means of the Wavelet Analyses Presented in Figure 1

Time Scale	Northern Hemisphere $B_{\rm avg}$ (days)	Southern Hemisphere $B_{\rm avg}$ (days)
Short-term periods	7.2	...
	9.3	9.1
	13.6	13.4
	27.7	27.2
Long-term periods	80	83
	161	149
	...	235
	409	321

Note. The periods of oscillations are obtained from the time series of the average Carrington latitude value $B_{\rm avg}$, in both the northern and southern hemispheres, for a time interval spanning from 2010 May 1 to 2014 December 31. The periods are expressed in days. The first column classifies the period (short vs. long). The remaining two columns yield information about the identified periods in the northern (second column) and southern (last column) hemispheres, respectively. The periods are estimated based on a 2σ (95%) confidence level.

of oscillation, we utilize the wavelet analysis software developed by C. Torrence & G. P. Compo (1998) to generate the wavelet power spectrum (WPS) of $B_{\rm avg}$, using the default Morlet wavelet profile. The WPS of $B_{\rm avg}$ for the northern and southern hemispheres can be seen in subpanel (II) of Figures 1(a) and (b), respectively. Next, we also calculated the associated global power spectrum (GPS) by accumulating the WPS (see, e.g., subpanel (III) of Figures 1(a) and (b)).

To determine the GLO periods found in the time series of $B_{\rm avg}$, we identified periodicities by inspecting the GPS and WPS plots with an applied 2σ significance for both of the hemispheres. The periods found are classified as short (from a few days to the length of the period of a CR) and long (periods well longer than a CR). For the actual values of these periods for each of the two hemispheres, see Table 1. The applied 2σ significance levels were based on a white-noise model and standard deviation of the input signals.

3.1. Global Latitudinal Short-period Oscillations

The short-term periods (i.e., shorter than or similar to the time needed for a CR) found are broadly similar in both hemispheres, with the exception of an additional 7.2 day period identified in the northern hemisphere only. The most prominent short-term period identified coincides with the 27.3 day CR (L. Svalgaard & J. M. Wilcox 1975; C. J. Henney & J. W. Harvey 2002; V. I. Haneychuk et al. 2003). This period supports the conjecture and is consistent with the presence of an active longitude, accepting that somewhere within this belt of longitudinal coordinates with higher solar activity there are active nests, as reported elsewhere (e.g., M. J. M. Castenmiller et al. 1986; M. P. Brouwer & C. Zwaan 1990; S. W. McIntosh et al. 2017).

Additionally, the harmonics of the $P_1 = {\sim}27.3$ day period are present too. Namely, periods of approximately $P_2 = {\sim}13.5$ days, $P_3 = {\sim}9$ days, and $P_4 = {\sim}7$ days are found. The ∼13.5 day periodicity is also reported by other researchers, e.g., when studying total UV irradiance and the projected areas of evolving complex group formations (R. F. Donnelly & L. C. Puga 1990; J. Pap et al. 1990; V. P. Bobova & N. N. Stepanian 1994). This biweekly periodicity is further established in the properties of the solar magnetic field in the observations from the Wilcox Solar Observatory (T. K. Das & T. K. Nag 1999) and by the Solar and Heliospheric Observatory (F. Boberg et al. 2002). The ∼13.5 day period may also be naturally accounted for by the presence of the active longitude phenomenon where "active nest" regions are present, as noted by M. J. M. Castenmiller et al. (1986) and G. de Toma et al. (2000).

Meanwhile, the ∼9 day cycle found here is also reported in other solar activities, e.g., it was linked to a triangular arrangement of coronal holes that are about 120° apart in longitude, as suggested by, e.g., S. R. Prabhakaran Nayar et al. (2001), M. Temmer et al. (2007), J. Lei et al. (2008), N. Ye et al. (2012), and P. Chowdhury et al. (2013).

The ∼7 day harmonic, along with other patterns like ∼27.3, 13.5, and 9 day oscillations, is often discussed in connection with solar wind and geomagnetic activity. This repeated geomagnetic activity, especially during periods of low solar activity, is proposed to be caused by fast solar-wind streams originating from large coronal holes and moving toward the Sun's equator, which interact with the Earth's magnetosphere (W. Wang et al. 2011; P. B. Kotzé 2015; J. Xu et al. 2015; J. Li et al. 2021, and references therein).

In summary, while the $P_1 = {\sim}27.3$ day and the $P_2 = {\sim}13.5$ day periods are consistent with the concept of active longitude, i.e., latitudinally concentrated active nests with a separation of 180°, the presence of the other two harmonics found may require further interpretation. The $P_3 = {\sim}9$ and $P_4 = {\sim}7$ day periods would align well with being higher harmonics if the system were an almost ideal resonator, i.e., where $P_n = P_1/n$ with $n = 2, 3,...$ an integer. Small deviations for a given mode from P_n, $n \geqslant 2$ may be used to determine diagnostic information about the inhomogeneities of the solar three-dimensional oscillator if at the above error level.

3.2. Global Latitudinal Long-period Oscillations

On the other hand, the lengths of the longer observed periods differ between the two hemispheres, unlike the shorter periods, which are more consistent. For instance, the periods of 80/161 and 83/149 days are similar in both hemispheres. However, for periods longer than 200 days, there are notable differences: the southern hemisphere has periods of 235 and 321 days, while the northern hemisphere has a longer period of 409 days.

4. Time-series Analyses of the Total Unsigned Facula Magnetic Flux in 5° Latitudinal Segments

To further explore how the previously identified short- and long-term periods are distributed as a function of the Carrington latitude in the northern and southern hemispheres, we determined the unsigned magnetic flux across a series of latitudinal segments binned in 5° latitudinal bands. The calculations were systematically performed on a bihourly basis, allowing for the generation of a detailed time-series data set. Next, similarly to Section 3, we applied wavelet spectrum analyses to the time series of the unsigned total magnetic flux of solar faculae, spanning from 2010 May 1 to 2014 December 31. The analysis encapsulated the magnetic activity manifesting across these 5° latitudinal binned segments, covering the entire range from the southern to the northern hemisphere.

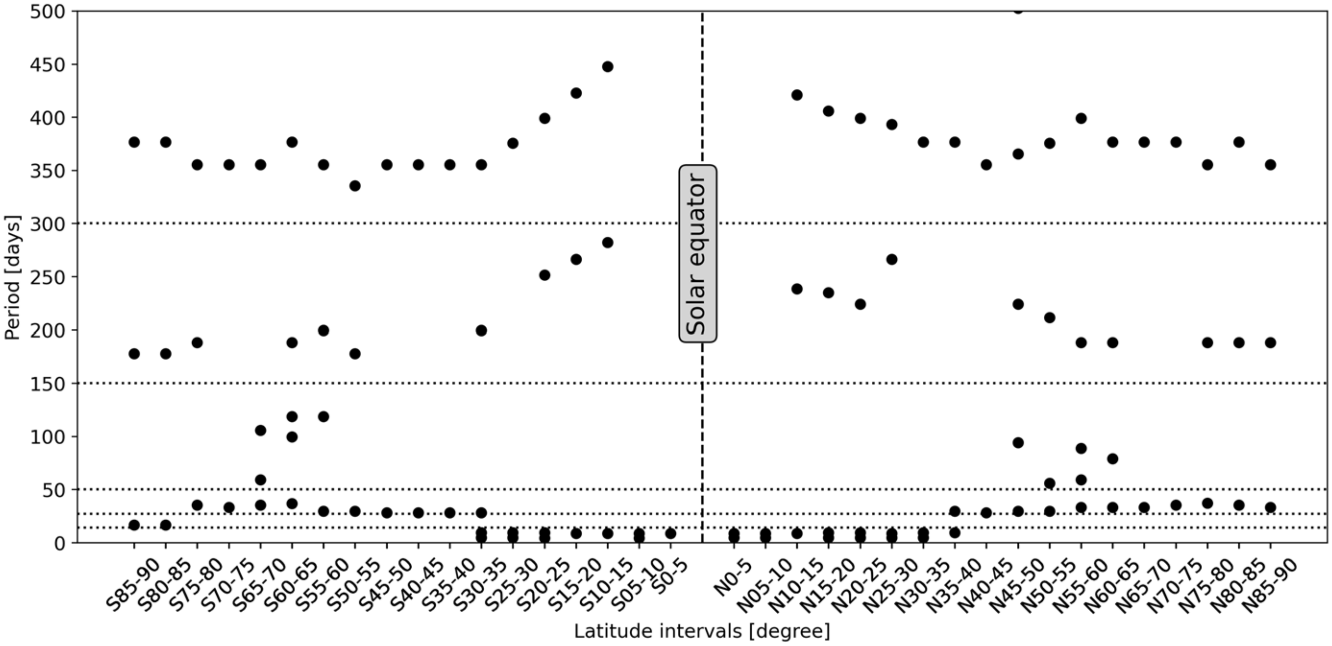

Figure 2. This plot shows the identified periods, with 2σ confidence, in the time series of the unsigned total magnetic fluxes of all faculae, recorded bihourly in binned 5° latitude segments. The y-axis represents the period in days, while the x-axis differentiates the binned latitude intervals in degrees, marked with "S" for southern and "N" for northern latitude segments. Horizontal dotted lines (at 13, 27, 50, 150, and 300 day periods) are provided as guides to help identify the different period intervals.

The periods identified in these 5° binned latitudinal segments are displayed in Figure 2. In this figure, the y-axis represents the period in days, while the x-axis differentiates the binned latitude intervals in degrees, clearly marked with "S" for southern and "N" for northern latitude segments. Our analysis of these hemispheric bands revealed some interesting and rather strong variations in the distribution of the periods in between the two poles, as follows:

1. Periods of ∼3–9 days are prominent between the S40 and N40 latitude bands only, corresponding to the presence of the well-known latitudinal solar-activity belt, where most solar activities, such as sunspots, solar flares, and faculae, are concentrated. These periods seem to also be harmonics of the ∼27.3 day CR. In fact, this (S40, N40) interval is the latitudinal range where the active longitude can be more distinctly identified (see, e.g., N. Gyenge et al. 2014).
2. In the latitudinal regions, farther away from the solar equator, spanning between S40–90 and N40–90, we identified oscillatory periods ranging between ∼13 and 35 days. These periods, as established in Section 3.1, also belong to the family of those that are associated with the CR and therefore the characteristic timescales of the differential rotational rate.
3. Next, within the S60–75 and N50–65 high-latitude bands, periods of ∼50–130 days can be observed. It is worth highlighting that these periods appear only in this narrow, ∼15° wide latitudinal band.
4. There is a discernible gradation within the ∼160–300 day range, where the periods found in the latitudinal bins gradually vary (decrease) from values about 300 to 160 days, as moving from the solar equator toward the polar regions, in both hemispheres. The periods sharply decrease in the solar-activity belt and remain relatively constant at higher latitudes.
5. Last but not least, a similar pattern of variation of periods is also apparent within the ∼300–500 day period range.
6. There is no clear or remarkable difference in the distribution of periods of latitudinal oscillations between the two hemispheres.

Based on the aforementioned findings, we can infer that the decrease in the magnitude of the observed latitudinal periodicities for periods greater than 150 days is strongest in the activity belt. Remarkably, this is also the region where the rotation rate of the differential rotation is not changing significantly (see Figure 1 in the review paper by J. G. Beck 2000). On the other hand, between $\sin B = (0.45–1)$, i.e., at higher latitudes where there is a significantly more pronounced variation in the differential rotational rate, the identified faculae daily averaged latitudinal periodicities may not seem to vary extensively as a function of latitude within the respective period bands, except for the one with the period range ∼50–150 days (see Figure 2).

5. On the Distribution of Faculae in Synoptic Maps

For the next stage of analysis, we focused on the synoptic maps of photospheric faculae for the interval epoch from 2010 May 1 to 2014 December 31, similar to G. de Toma et al. (2000), who analyzed the Sun's magnetic field synoptic maps from 1996 to 1998. For the duration of this ∼4.5 yr, the analyzed synoptic maps were sourced from the SDO/HMIDD catalog, as visualized in Figures 3–4.

The left panels of Figures 3–4 display the series of synoptic maps of solar faculae for CRs 2113–2130. Red points represent faculae with positive magnetic field values, while blue points indicate faculae with negative ones.

The right panels of Figures 3–4 present the corresponding contour maps, generated from the solar faculae synoptic maps. These contour maps are the result of applying the density-based

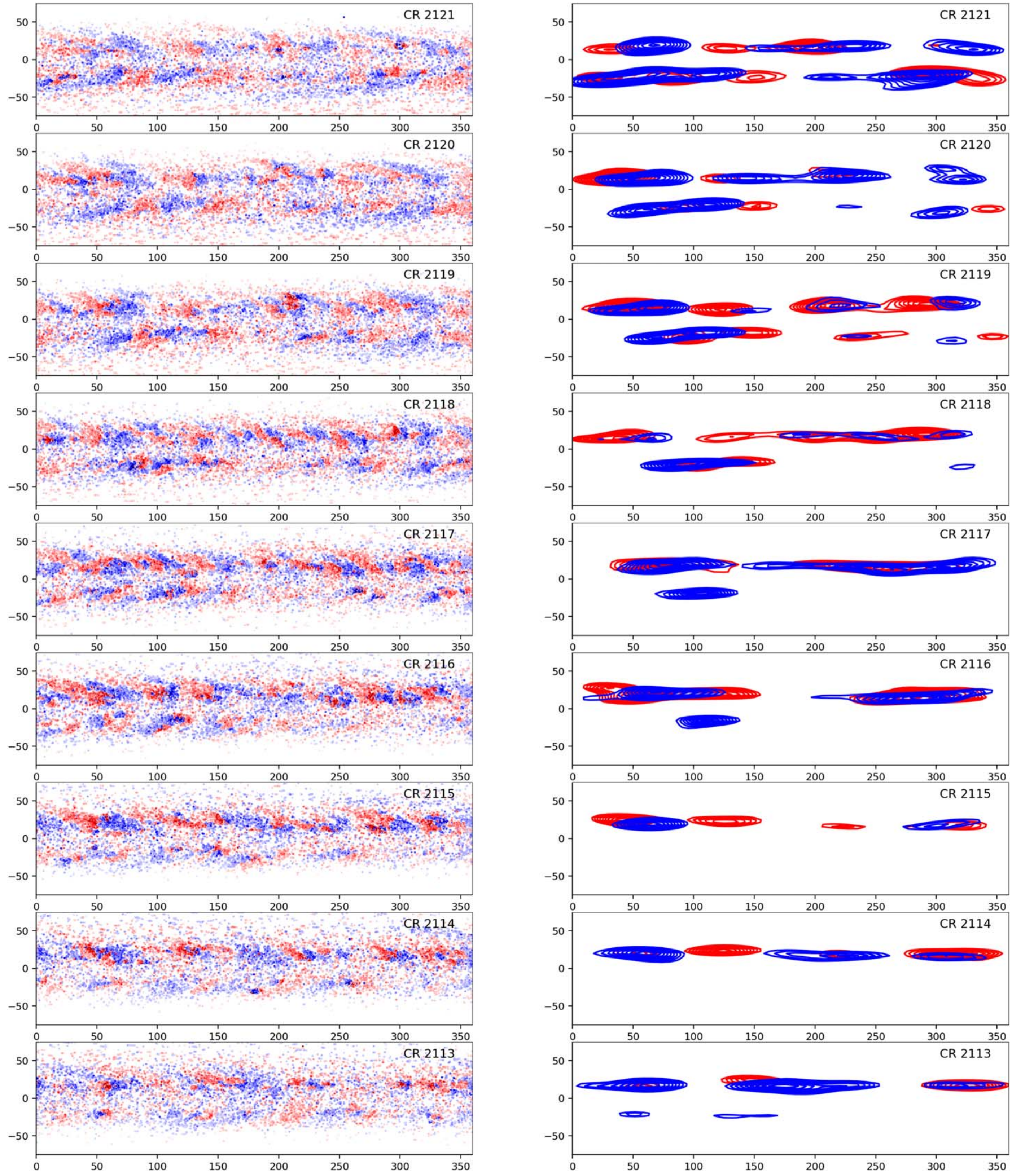

Figure 3. Solar faculae in Carrington maps for CR 2113-2121 (left panel) with red and blue colors denoting positive and negative magnetic fields, respectively. The right panel shows contour maps derived from the CR map data employing the DBSCAN and KDE methods.

spatial clustering of applications with noise (DBSCAN; M. Ester et al. 1996) and kernel density estimation (KDE; S. J. Sheather 2004) techniques. With the DBSCAN algorithm, we cluster the positive and negative faculae separately based on their spatial coordinates. First, this clustering algorithm identifies the maximum distance (here, 1°) between two faculae to be considered neighbors and the minimum number of the faculae. A minimum sample size of 10 faculae was considered,

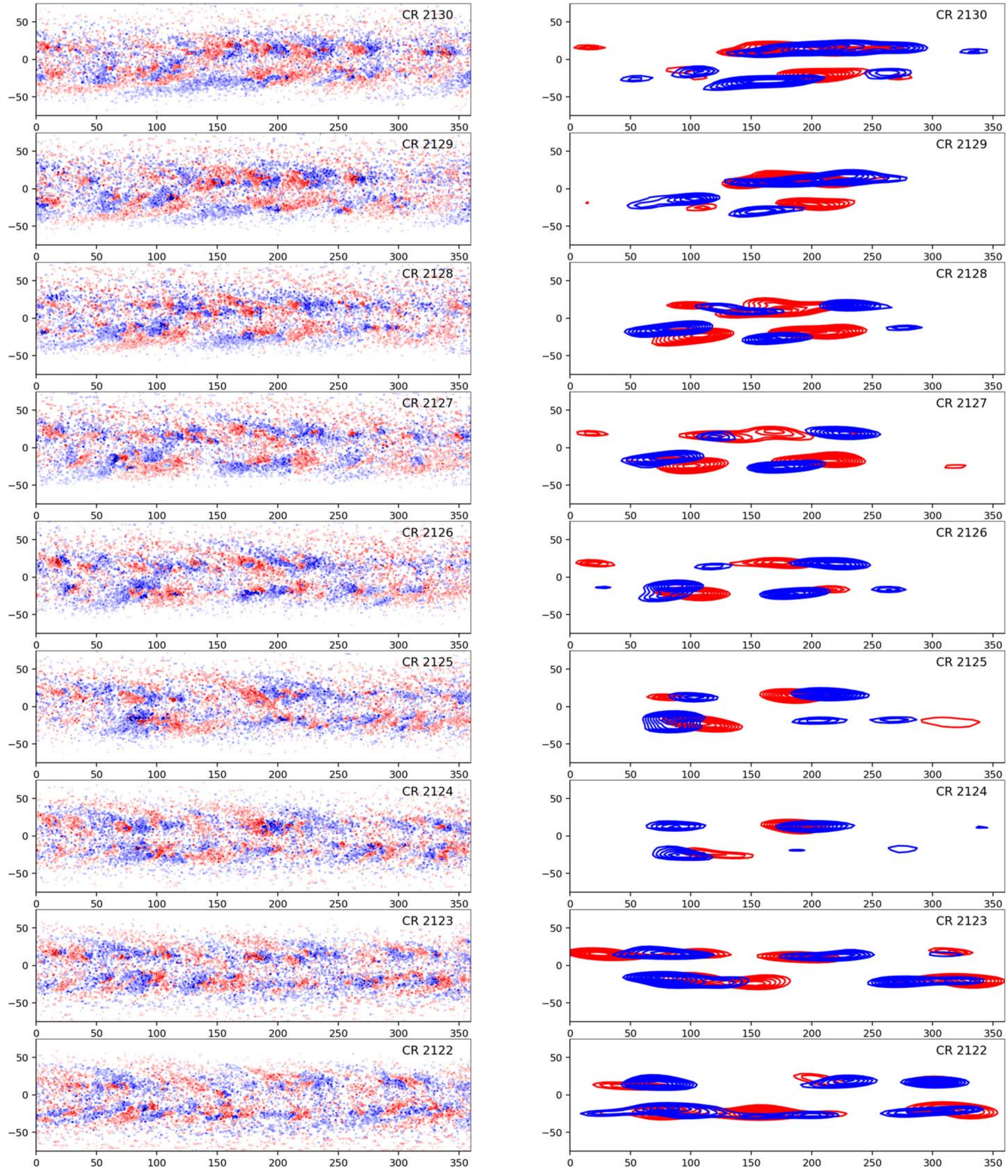

Figure 4. This figure is similar to Figure 3, but in this case, it represents the Carrington maps for CR 2122-2130.

as it was found to be the most suitable choice after several tests. Next, KDE is used to estimate the probability density function (PDF) of each cluster. KDE is a nonparametric method that relies on a Gaussian kernel to smooth the faculae data points and approximates the underlying distribution of them in each cluster. The Gaussian kernel function assigns weights to nearby faculae based on their distance, with larger weights for closer faculae and smaller weights for more distant ones. The

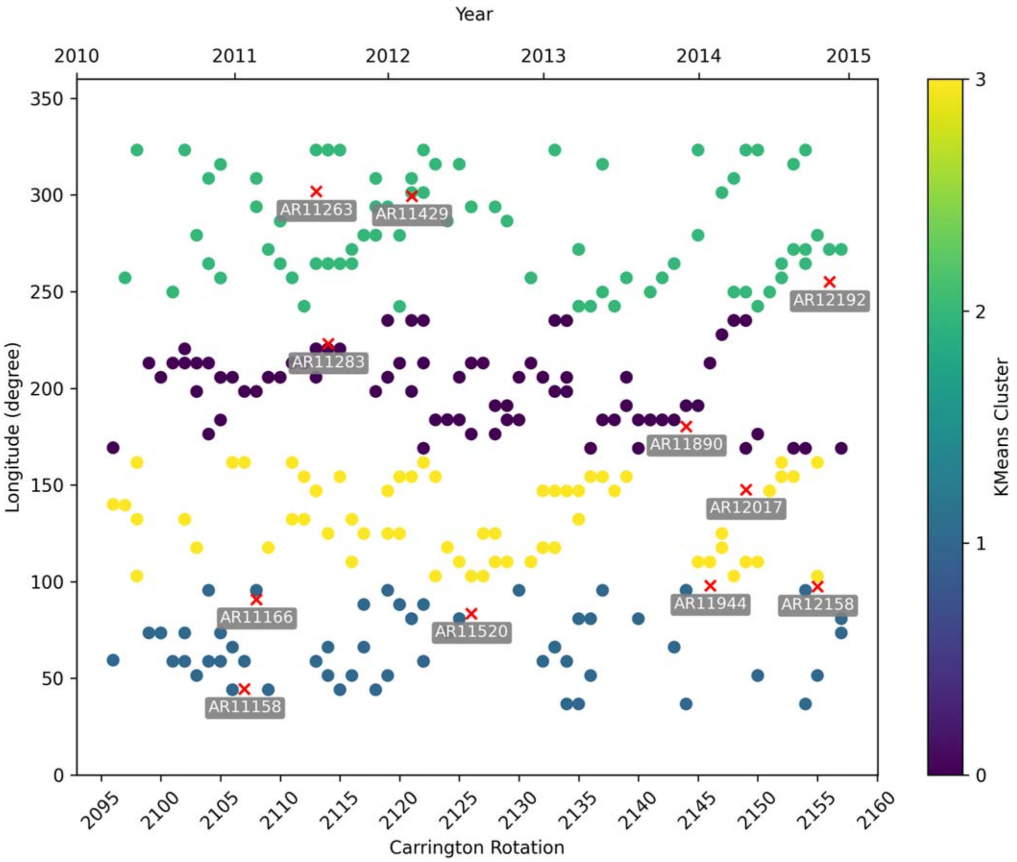

Figure 5. Illustrating the longitudinal positions of solar faculae as tracked over successive CRs. These positions are clustered using a K-means algorithm. The color bar indicates the classification order of the identified longitudinal clusters. Next, active regions that produced X-class flares during the investigated 4.5 yr interval are overplotted. The red crosses represent the positions of these active regions in CRs (i.e., time).

aggregate of these weighted contributions results in a smooth curve that approximates the PDF.

Next, the contour levels in the right panels of Figures 3–4 are determined based on the PDF values to ensure that the contours encompass the most significant or populated regions of the faculae with the respective positive and negative magnetic fields. Red/blue contours denote areas with a higher density of positive/negative magnetic field values. Ultimately, the calculated centroids of the "positive" and "negative" clusters yield the Carrington longitude and latitude coordinates, which then serve as the central points of the identified facula clusters for subsequent analysis. Let us now investigate the longitude coordinates of these calculated centroids.

To analyze the longitudinal distribution of the most significant or densely populated facula regions, we plot the centroid longitudinal coordinates of the positive and negative clusters as a function of CR in Figure 5. Subsequently, we apply a K-means clustering algorithm (J. A. Hartigan & M. A. Wong 1979) to determine the nonuniform distribution, if any, of the longitudinal coordinates shown in Figure 5. The K-means algorithm itself partitions a data set into distinct groups or clusters based on similarity, assigning data points to the nearest cluster center and aiming to minimize variance within each cluster. This iterative process continues until the cluster centers stabilize, grouping the data into coherent, nonoverlapping subsets.

During the K-means clustering classification analysis, we evaluated various cluster configurations ($n = 1$ to 10), while concurrently using the analysis of variance (ANOVA) statistical validation technique (A. Gelman 2005) to confirm the significance of differences between clusters and their alignment with latitudinal positions within our existing K-means model. Based on the ANOVA results, the configuration with four clusters ($n = 4$) was identified as statistically significant. This suggests that the differences between the clusters reflect actual variations in the underlying longitudinal distribution.

The K-means method, as applied, identified four distinct clusters of longitudinal coordinates, presented in Figure 5. Each cluster is color-coded in accordance with the algorithm's classification sequence, as marked on the color bar on the right-hand side. Cluster 0 (dark purple) encompasses longitudes between 170° and 240°. Cluster 1 (dark blue) is found between 40° and 100°, Cluster 2 (green) spreads out between 240° and 330°, and Cluster 3 (yellow) stretches between 100° and 170°. Clusters 1 and 2 exhibit a wider population compared to Clusters 0 and 3. The centers of Clusters 1 and 2 are about 180° apart, which is consistent with the notion of the existence of a pair of active longitudes.

Upon closer visual inspection of Figure 5, we identified subclasses within each of the four main clusters that might be described as active nests. These active nests seem to appear preferentially within the active longitudes that persist throughout the lifespans of specific active longitudes (M. Ternullo 2010). For example, potential active nests were observed within the ranges of CR 2095–2110, CR 2112–2134, and CR 2135–2150 in Cluster 0. These active nests typically persist for about 15–20 CR, equivalent to approximately 409–546 days. We overlaid the positions of solar active regions that hosted the largest intensity-class flares (X-class flares) during the studied period, as a preliminary step. These regions are marked with red crosses and labeled with their NOAA identification numbers in Figure 5. Interestingly, upon visual inspection, these active regions tend to be located toward the middle or end of some of the identified active nests. This observation tentatively suggests that from the middle to the end of an active nest's life cycle, we might expect the emergence of magnetically complex active regions capable of producing significant solar eruptions. However, this conjecture about the connection between active nests on active longitudes and intense flare activity requires further detailed analysis in the near future.

6. Conclusions

This study builds on the research conducted by A. Elek et al. (2024), which involved a thorough analysis of the SDO/HMIDD catalog from 2010 May 1 to 2014 December 31 (T. Baranyi et al. 2016). An important discovery made by A. Elek et al. (2024) was the detection of alternating strong and weak longitudinal facula bands at lower solar latitudes. The presence of these alternating bands lends support to the debated notion of the active longitude pair. A. Elek et al. (2024) strengthened this hypothesis by employing a visual heuristic model and supporting additional advanced dynamo simulations, thus enhancing our comprehension of this solar active longitude phenomenon.

A. Elek et al. (2024) also briefly reported various oscillatory patterns identified by means of a fast Fourier transform of the loci of faculae. They noted that solar quasi-biennial oscillations, with durations ranging from 0.3 to 2 yr, were particularly prominent. Additionally, they have also detected shorter activity cycles, lasting merely 4–12 days and primarily at latitudes between –45° and 45°, that potentially may connect to a pair of active longitudes. However, they did not explore the relationships among these various periods. Therefore, in order to fill this gap, our study now aims to delve deeper into these periods.

Initially, our analysis considered every 2 hr data from 2010 May 1 to 2014 December 31. For this, we determined the mean Carrington latitude value, $B_{\rm avg}$, for all faculae per observations for both hemispheres. This enabled conducting separate wavelet analyses for the northern and southern hemispheres, as depicted in Figure 1. Our findings, detailed in Table 1, revealed both short- and long-term periodicities in each hemisphere. The results are as follows:

1. Notably, the periodicities found of short-term cycles were similar across both hemispheres, with a prominent period of ∼27.3 days matching the Carrington period. Additionally, we noted higher harmonics of this characteristic period, with approximately 13.5 and 9 day cycles in both hemispheres, potentially linking them to the presence of active nests in active longitudes, as suggested by M. J. M. Castenmiller et al. (1986), G. de Toma et al. (2000), and A. Elek et al. (2024).
2. Meanwhile, the long-term periods, between ∼80 and 409 days, showed more hemispheric variations when compared to their short-term period counterparts, as outlined in Table 1.

In order to deepen our comprehension of the distribution of short- and long-term periodicities in facula loci time series across different latitudes, we carried out wavelet spectrum analysis of the unsigned magnetic flux. This analysis was performed within a series of 5° latitudinal bands piling up consecutively from the southern –90° to the northern 90° latitude. The resulting periods of oscillations are identified within these 5° segments:

1. The ∼3–9 day periods were notably prominent within the lower latitudinal band, between S40 and N40 degrees. Within the higher latitudinal zones, spanning S40–90 and N40–90, we observed periods of ∼13 and 35 days. Additionally, in the S60–75 and N50–65 high-latitude bands, we detected periods ranging from about 50 to 130 days (see in Figure 2).
2. Regarding the identified longer than 130 day periods, a gradual decrease in the length of the periods was reported: from approximately 300 to 160 days and from 500 to 300 days, when sampling from the equatorial region toward the poles in both hemispheres (as illustrated in Figure 2).

To investigate the presence of active longitude, we further explored and built upon the approach by G. de Toma et al. (2000). Our objective was to analyze whether there is a significant concentration of positive and negative magnetic polarity faculae in the synoptic maps of the observed ∼4.5 yr interval. To accomplish this, the DBSCAN and KDE methods were utilized. Next, the longitude and latitude centroids of the identified positive and negative magnetic polarity facula clusters were determined. Finally, the temporal distribution of the longitudinal central coordinates, employing the K-means clustering algorithm, was established, as illustrated in Figure 5. We found as follows:

1. There are four distinct groups, called clusters, of longitudinal coordinates organized into two pairs: Clusters 0 and 1 make up the first pair, and Clusters 2 and 3 form the second pair. Each pair is separated by about 180°, being consistent with the presence of active longitude pairs. Within each individual group, active nests were identified, usually lasting around 15–20 CR, or ∼410–550 days.
2. Notably, the host active regions of the most energetic solar eruptions appear to be predominantly in the middle or at the end of the lifetime of an active nest.

Specifically, the presence of an active nest on active longitude raises one's anticipation that one could expect the emergence of magnetically complex active regions that could produce major solar eruption(s). An active nest at an active longitude may suggest its potential role as a warning sign of major solar eruption activity over week-long timescales (M. Dikpati et al. 2021 and references therein). The active longitude appears to bridge the gap in the prediction of the various wider-scale timelines, connecting longer-term forecasts with shorter-term (hours to days) predictions.

Additional research is therefore needed to validate these hypotheses and deepen our understanding of the relationship between the active longitude, active nests, and large eruptions produced by magnetically complex active-region appearances. To this end, a natural extension of this investigation through a similar analysis of a series of magnetic synoptic maps would be encouraged, with a focus on establishing the temporal variation and evolution of the active longitude. If found, this would then have rather important implications for dynamo theory, which could make a leap forward in the modeling of three-dimensional nonaxisymmetric approaches to the dynamic solar interior.

Acknowledgments

M.B.K. is grateful for the Leverhulme Trust Fund ECF-2023-271. M.K.B. acknowledges ÚNKP-23-4-II-ELTE-107, ELTE Hungary. M.B.K., F.Z., and R.E. acknowledge support from the European Union's Horizon 2020 research and innovation program under the grant agreements No. 739500 (PRE-EST project) and No. 824135 (SOLARNET project). M.B.K. and F.Z. acknowledge support by the Università degli Studi di Catania (PIA.CE.RI. 2020-2022 Linea 2), by the Italian MIUR-PRIN grant 2017APKP7T, and by the CAESAR ASI-INAF n. 2020-35-HH.0 project. R.E. and M.B.K. are grateful for the support received from NKFIH OTKA (Hungary, grant No. K142987) and from ISSI-BJ ("Step forward in solar flare and coronal mass ejection (CME) predicting"). R.E. is grateful to STFC (UK, grant No. ST/M000826/1) and PIFI of the Chinese Academy of Sciences (grant No. 2024PVA0043). This work was also supported by the NKFIH Excellence Grant TKP2021-NKTA-64.

ORCID iDs

Marianna B. Korsós https://orcid.org/0000-0002-0049-4798
Anett Elek https://orcid.org/0000-0003-3379-0988
Francesca Zuccarello https://orcid.org/0000-0003-1853-2550
Robertus Erdélyi https://orcid.org/0000-0003-3439-4127

References

Bai, T. 1988, ApJ, 328, 860
Bai, T. 2003, ApJ, 585, 1114
Balthasar, H. 2007, A&A, 471, 281
Baranyi, T., Győri, L., & Ludmány, A. 2016, SoPh, 291, 3081
Beck, J. G. 2000, SoPh, 191, 47
Benevolenskaya, E. E., Kosovichev, A. G., & Scherrer, P. H. 1999, SoPh, 190, 145
Berdyugina, S. V., & Usoskin, I. G. 2003, A&A, 405, 1121
Boberg, F., Lundstedt, H., Hoeksema, J. T., Scherrer, P. H., & Liu, W. 2002, JGRA, 107, 1318
Bobova, V. P., & Stepanian, N. N. 1994, SoPh, 152, 291
Bogart, R. S. 1982, SoPh, 76, 155
Bovelet, B., & Wiehr, E. 2001, SoPh, 201, 13
Brouwer, M. P., & Zwaan, C. 1990, SoPh, 129, 221
Bumba, V., Garcia, A., & Klvaňa, M. 2000, SoPh, 196, 403
Bumba, V., & Howard, R. 1969, SoPh, 7, 28
Castenmiller, M. J. M., Zwaan, C., & van der Zalm, E. B. J. 1986, SoPh, 105, 237
Chowdhury, P., Jain, R., & Awasthi, A. K. 2013, ApJ, 778, 28
Das, T. K., & Nag, T. K. 1999, SoPh, 187, 177
de Toma, G., White, O. R., & Harvey, K. L. 2000, ApJ, 529, 1101
Dikpati, M., McIntosh, S. W., Chatterjee, S., et al. 2021, ApJ, 910, 91
Donnelly, R. F., & Puga, L. C. 1990, SoPh, 130, 369
Elek, A., Korsós, M., Dikpati, M., et al. 2024, ApJ, 964, 112
Ester, M., Kriegel, H.-P., Sander, J., & Xu, X. 1996, in Proc. Second Int. Conf. on Knowledge Discovery and Data Mining, KDD'96, ed. E. Simoudis, J. Han, & U. Fayyad (Palo Alto, CA: AAAI Press), 226
Frazier, E. N. 1971, SoPh, 21, 42
Gaizauskas, V., Harvey, K. L., Harvey, J. W., & Zwaan, C. 1983, ApJ, 265, 1056
Gelman, A. 2005, Ann. Statist., 33, 1
Gyenge, N., Baranyi, T., & Ludmány, A. 2014, SoPh, 289, 579
Gyenge, N., Ludmány, A., & Baranyi, T. 2016, ApJ, 818, 127
Györi, L. 1998, SoPh, 180, 109
Haneychuk, V. I., Kotov, V. A., & Tsap, T. T. 2003, A&A, 403, 1115
Hartigan, J. A., & Wong, M. A. 1979, JSTOR: Appl. Statist., 28, 100
Henney, C. J., & Harvey, J. W. 2002, SoPh, 207, 199
Heristchi, D., & Mouradian, Z. 2009, A&A, 497, 835
Juckett, D. A. 2006, SoPh, 237, 351
Kostyuchenko, I. G., & Vernova, E. S. 2024, Ge&Ae, 63, 1210
Kotzé, P. B. 2015, AnGeo, 33, 31
Lei, J., Thayer, J. P., Forbes, J. M., Sutton, E. K., & Nerem, R. S. 2008, GeoRL, 35, L10109
Li, J., Wang, S., Li, S., Xu, Z., & Yang, J. 2021, Ap&SS, 366, 73
Losh, H. M. 1939, POMic, 7, 127
McIntosh, S. W., Cramer, W. J., Pichardo Marcano, M., & Leamon, R. J. 2017, NatAs, 1, 0086
Mursula, K., & Hiltula, T. 2004, in 35th COSPAR Scientific Assembly (Paris: ESA), 2817
Pap, J., Tobiska, W. K., & Bouwer, S. D. 1990, SoPh, 129, 165
Pelt, J., Korpi, M. J., & Tuominen, I. 2010, A&A, 513, A48
Prabhakaran Nayar, S. R., Sanalkumaran Nair, V., Radhika, V. N., & Revathy, K. 2001, SoPh, 201, 405
Ruzmaikin, A., Feynman, J., Neugebauer, M., & Smith, E. J. 2001, JGR, 106, 8363
Schwabe, H., & Schwabe, H. 1844, AN, 21, 233
Sheather, S. J. 2004, StaSc, 19, 588
Svalgaard, L., & Wilcox, J. M. 1975, SoPh, 41, 461
Temmer, M., Vršnak, B., & Veronig, A. M. 2007, SoPh, 241, 371
Ternullo, M. 2010, Ap&SS, 328, 301
Title, A. M., Topka, K. P., Tarbell, T. D., et al. 1992, ApJ, 393, 782
Torrence, C., & Compo, G. P. 1998, BAMS, 79, 61
Usoskin, I. G., Berdyugina, S. V., & Poutanen, J. 2005, A&A, 441, 347
Wang, W., Lei, J., Burns, A. G., et al. 2011, SoPh, 274, 457
Xu, J., Wang, W., Zhang, S., Liu, X., & Yuan, W. 2015, JGRA, 120, 3829
Ye, N., Zhu, F. R., Zhou, X. M., & Jia, H. Y. 2012, SoPh, 279, 411
Zhang, L., Mursula, K., Usoskin, I., & Wang, H. 2011, A&A, 529, A23